



## Finite element simulations of conjugate heat transfer of non-Newtonian fluids in a porous cavity having circular heated blocks

Journal:	<i>Science Progress</i>
Manuscript ID	SCI-25-1519
Manuscript Type:	Original Research Article
Date Submitted by the Author:	09-Jul-2025
Complete List of Authors:	Ahmad, Siddeeq ; University of Science & Technology Bannu Jan, Hameed Ullah ; University of Science & Technology Bannu Ahmad, Shafee; Jiangsu University Khan, Zeeshan; Bacha Khan University Charsadda Khan, Waris; Hazara University, Shah, Bashir ; King Saud University College of Engineering
Keywords:	Conjugate heat transfer, Nusselt number, Sherwood number, Kinetic energy, Entropy generation, Bejan number
Abstract:	<p>The conjugate heat transfer is more significant and realistic in a variety of engineering applications. This study aims to investigate conjugate heat transfer and fluid flow phenomena in a square cavity within the non-homogeneous mixture of Nanoparticles. Four exothermic circles are clustered at each vertex of the cavity. Two cases, Case A and Case B, based on boundary conditions, are discussed in detail. The study explores the influence of non-dimensional parameters on system dynamics by analyzing the velocity field, heat flow, and mass transport. Utilizing the Finite element method, the partial differential equations are solved, and simulations are conducted with varying Rayleigh (Ra), Lewis (Le), Hartmann (Ha) and Darcy numbers (Da). The influence of these parameters are carefully investigated on mean Nusselt (Nu<sub>avg</sub>) and Sherwood numbers (Sh<sub>avg</sub>). Streamlines, isotherms and iso-concentration effects are visualized qualitatively. The increase in Da and Ha leads to decrease in the Nu<sub>avg</sub> and Sh<sub>avg</sub>. The Nu<sub>avg</sub> is changed from 4.9717 to 5.0112 with from horizontal to vertical. Insignificant effect of AR is seen on Nu<sub>avg</sub> and 1.13% decrease is calculated by changing it from 0.05 to 1, in case A. Increasing Le results in higher Nu<sub>Local</sub> and Sh<sub>Local</sub>.</p>

SCHOLARONE™  
Manuscripts

**Finite element simulations of conjugate heat transfer of non-Newtonian fluids in a porous cavity having circular heated blocks**

**Siddeeq Ahmad<sup>1</sup>, Hameed Ullah Jan<sup>1</sup>, Shafee Ahmad<sup>2</sup>, Zeeshan Khan<sup>3</sup>, Waris Khan<sup>4,\*</sup>, Bashir Shah<sup>5</sup>**

<sup>1</sup>Department of Mathematics, University of Science and Technology Bannu , Pakistan

<sup>2</sup>School of Energy and Power Engineering, Jiangsu University Zhenjiang, 212013, China

<sup>3</sup>Department of Mathematics and Statistics, Bacha Khan University Charsadda, KP, Pakistan

<sup>4</sup>Department of Mathematics & Statistics, Hazara University, Mansehra, 21120, Khyber Pakhtunkhwa, Pakistan

<sup>5</sup>Department of Industrial Engineering, College of Engineering, King Saud University, Riyadh 12372, Saudi Arabia

\*Corresponding author: (wariskhan758@yahoo.com)

**Abstract:** The conjugate heat transfer is more significant and realistic in a variety of engineering applications. This study aims to investigate conjugate heat transfer and fluid flow phenomena in a square cavity within the non-homogeneous mixture of Nanoparticles. Four exothermic circles are clustered at each vertex of the cavity. Two cases, Case A and Case B, based on boundary conditions, are discussed in detail. The study explores the influence of non-dimensional parameters on system dynamics by analyzing the velocity field, heat flow, and mass transport. Utilizing the Finite element method, the partial differential equations are solved, and simulations are conducted with varying Rayleigh ( $Ra$ ), Lewis ( $Le$ ), Hartmann ( $Ha$ ) and Darcy numbers ( $Da$ ). The influence of these parameters are carefully investigated on mean Nusselt ( $Nu_{avg}$ ) and Sherwood numbers ( $Sh_{avg}$ ). Streamlines, isotherms and iso-concentration effects are visualized qualitatively. The increase in  $Da$  and  $Ha$  leads to decrease in the  $Nu_{avg}$  and  $Sh_{avg}$ . The  $Nu_{avg}$  is changed from 4.9717 to 5.0112 with  $\gamma$  from horizontal to vertical. Insignificant effect of  $AR$  is seen on  $Nu_{avg}$  and 1.13% decrease is calculated by changing it from 0.05 to 1, in case A. Increasing  $Le$  results in higher  $Nu_{Local}$  and  $Sh_{Local}$ .

**Keywords:** Conjugate heat transfer; Nusselt number; Sherwood number; Kinetic energy; Entropy generation; Bejan number

**1. Introduction**

Conjugate heat transfer in a variety of geometries has drawn a lot of interest recently since it is important for comprehending thermal behavior and streamlining heat exchange procedures. Conjugate heat transfer is a more realistic depiction of thermal processes in real life because it considers both heat convection and conduction in solids at the same time. Applications for this

multidisciplinary field can be found in environmental science, engineering, and physics, among other fields. Understanding complex fluid dynamics in the presence of obstacles is critical to improving system performance and reducing energy loss. In the previous decade, numerous research studies have explored various aspects aimed at enhancing the technique of heat transfer [1-2]. Their investigations show that adding nanoparticles increases its thermal conductivity, impacting the convection phenomenon. Furthermore, a slim fin was connected to the heated left wall. Numerous studies have examined the impact of fin attachments on natural convection within the cavity [3-6]. The effects of T-shaped object in permeable enclosure has been studied by Hatami et al. [7]. They investigated that Darcy and porosity have direct relation with heat transfer. Dash et al.'s study [8] examined the effects of Casson flows on porous medium pipes in order to shed light on the special traits and behaviours connected to these intricate fluid systems. The first person to talk about the entropy caused by heat transfer and flow friction was Bejan [9]. Furthermore, as discussed in [10], the thermodynamic approach's entropy generation minimization contributes to increased energy efficiency. Second-law analysis, also known as the minimization of entropy, can be used to improve the efficiency of several systems, including diesel engines, thermal storage, and reactors [11-13]. Basak and others [14] looked at the entropy generation of free convection flow in the cavity under a variety of thermal conditions and with various walls. The entropy generation of hybrid Nanofluid, non-uniform heat generation, and impact of Darcy–Forchheimer Model were deeply analyzed [15-18]. Eckert number showed direct impact with the enhancement of temperature. It was obtained that porous parameter retarding the fluid velocity. The magnetic parameter showed that as one increases it, the fluid velocity decreases and temperature increases. Reddy and Sreedevi [19] recently investigated the effects of thermal radiation on entropy generation and thermal transport in an electromagnetic hybrid nanofluid saturation in a square enclosure. They discovered that silver nanoparticles have a higher rate of energy transport than copper nanoparticles do. Jan et al. [20] investigated Reiner–Philippoff based nanofluid for thermal transportation with effects of viscous dissipation. They obtained that Lorentz force can produce resistance and entropy is generated. The curvature effects was analyzed and found that it has an inverse relation with heat flow. Dutta et al. [21] investigated how fluid flow was affected by heat transport, entropy production, and MHD. They discovered that the Hartmann number decreases significantly with the thermal transmission rate at high Rayleigh numbers ( $Ra > 10^5$ ). Bondareva et al. [22] showed that a bent porous nook's shape, game plan, and Hartmann number

could impact heat transmission characteristics. Further significant works on MHD in an enclosure can be found in references [23-26]. Kotha et al. [27] The authors emphasise the importance of their investigation into entropy generation for a Casson fluid with viscous dissipation on a heated surface in the improvement and optimisation of energy systems. Consequently, Shaw et al. [28] used the Darcy-Forchheimer model to study the dynamic behaviour of the brain on a rotating disc, paying particular attention to the consequences of entropy generation. Adebayo et al. [29] analysed entropy generation with thermal radiation influence was carried out using numerical techniques. An artificial neural network (ANN) approach was adopted to optimize the impact of hybrid Nanofluid on heat and mass flow [30, 32]. It was observed that heat is improved by adding nanoparticles. It was further examined that Darcy's dissipation significantly affects the flow variables. The response surface methodology optimizes the velocity and heat phenomenon in a better way. Results showed that interactions of magnetic field and thermal radiation impact rate of heat transfer and entropy generation. Rupa et al. [33] studied the effects of homogeneous-heterogeneous reactions of micropolar nanofluid for energy transport and velocity field. It was observed that particle concentration gives rise to augmentation of axial velocity and temperature. The Casson fluid with effects of bioconvection of nanofluid for cooling system was examined by Reddy and Baithalu [34, 35]. Their outcomes presented that velocity retarded with the increase of Casson parameter. The magnetic parameter showed that as one increases it, the fluid velocity decreases and temperature increases. Shamshuddin et al. [36] methods for analysing the Casson fluid under the influence of both electric and Hall currents were investigated using the Finite Element Method (FEM). Goud et al. [37] FEM was also utilised for the analysis of oscillating plates that contained MHD Casson fluids. likewise, Majeed et al. [38] investigated simulations using the finite element method (FEM) with higher-order techniques on Casson fluids in relation to heat transfer. Khader et al. [39] investigated numerical techniques for the analysis of unsteady Casson fluid behaviour using the Finite Element Method (FEM), exploring the multiscale stabilisation features of non-Newtonian Casson fluid in rectangular cavities by Kumar et al. [40]. As a result, there has been a growing focus on studying conjugate heat transfer in recent times. For example, Zhao *et al.*, [41] examined how placing a conductive wall at various locations within a cavity affects both fluid flow and the heat transfer rate (HTR). The research has also been expanded to investigate the effect of sinusoidal heating on the right wall, incorporating a centrally positioned conductive block [42]. Subsequently, Chamkha and Ismael [43] employed the finite difference

method to investigate the impact of a porous medium and a triangular solid wall on the flow pattern of nanoliquid. Their study also explored the associated heat transfer rates at the interface and within the nanoliquid region. Ismael and Chamkha [44] conducted a numerical study to explore how solid, porous, and nanoliquid layers affect fluid flow and thermal fields. Additionally, they carried out a comparative analysis of heat transfer rates (HTR) using various nanoliquid models with different thermal conductivity and viscosity properties. Garoosi and Talebi [45] conducted a thorough numerical investigation into conjugate free and mixed nano liquid convective flow as well as heat transfer enhancement in a cavity with varying numbers and positions of conductive walls and hot/cold blocks. In their study, they pinpointed a critical nanoparticle concentration required to achieve higher heat transfer rates for a specified nanoparticle diameter. Mehryan *et al.* [46] investigated the flow of nanoliquid and heat transfer characteristics in a partially heated cavity. The cavity consisted of three distinct layers: a solid region, a porous medium, and nano liquid. Buongiorno's and Linear Thermal Non-equilibrium (LTNE) models were employed to analyze the behavior of the system.

This work explores the combined effects of fluid rheology and obstacles on entropy generation, focusing on Casson fluids. The study of fluid dynamics is essential to comprehending how fluids behave under various circumstances. The thorough investigation and comprehension of Newtonian fluids have made it possible to delve further into the study of non-Newtonian fluids, particularly those that display yield stress. These fluids offer intriguing challenges as well as a wide range of application possibilities.

## 2. Problem formulation

The problem under investigation is shown in Figure 1. We consider a two-dimensional square cavity of length ( $L$ ) with four circular cylinders placed diagonally at the corners. The diameter of each circular cylinder is equal to  $0.1L$ . An endothermic rectangular cylinder, whose length is  $0.4L$  and whose variable width is varied according to the aspect ratio ( $AR = 0.025$  to  $1$ , with varying increment sizes), is positioned in the center. Two cases are considered for center rectangular object, case A and case B. In case A, the object is conductive and heat loss through the vertical cavity wall. In case B, it is isothermal having a lower temperature,  $T_c^*$ . In addition, at an angle with horizontal axis, a magnetic field of strength  $B_0$  is applied. All of the cavity's walls are subjected to adiabatic conditions with no-slip velocity, and a rectangular block with lower temperature and concentrations of  $(T_c^*)$  and  $(c_c^*)$  coexists with circular cylinders that are kept at a higher

temperature ( $T_h^*$ ) and a greater mass concentration ( $c_h^*$ ). There is a non-Newtonian Casson fluid inside this enclosure. It is assumed that the flow is laminar, incompressible, uniform, and steady-state. The effects of viscous dissipation, Soret and Duffer effects are considered to be negligible. Moreover, the variation in density due to temperature differences can happen only in gravitational acceleration terms. The fluid properties are taken to be constant. The conservation of mass, momentum, energy, and concentration are all included in the governing equations for this situation. Below are the boundary conditions that go with it.

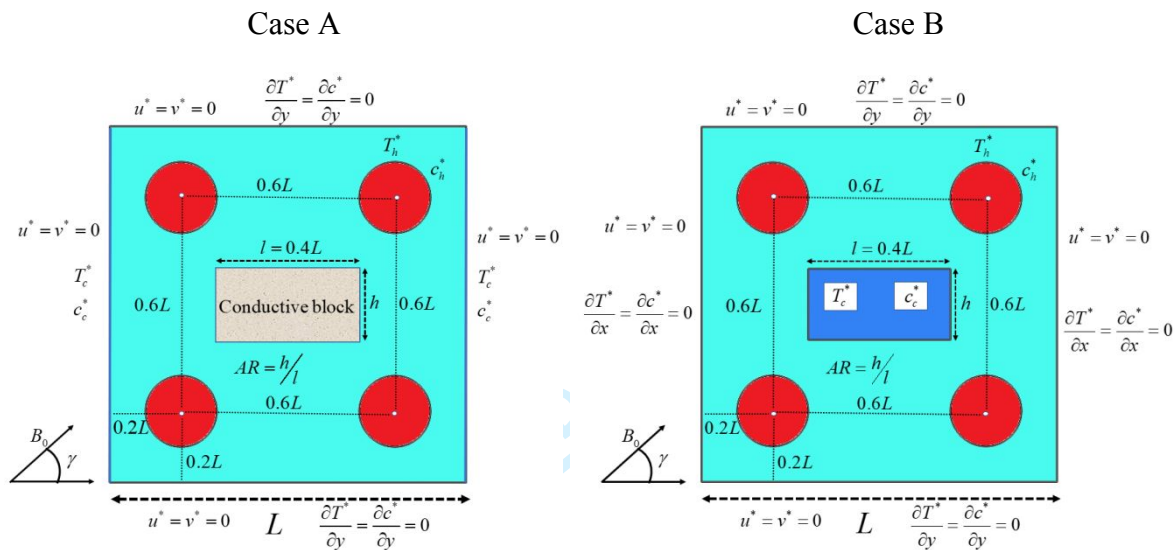


Figure 1. Geometry of the proposed problem.

$$u_x^* + v_x^* = 0 \quad (1)$$

$$u^* u_x^* + v^* u_y^* = -\frac{1}{\rho} p_x^* + v \left( 1 + \frac{1}{\beta} \right) (u_{xx}^* + u_{yy}^*) - \frac{v}{K} u^* + \frac{1}{\rho} \sigma B_0^2 (v^* \sin \gamma \cos \gamma - u^* \sin^2 \gamma) \quad (2)$$

$$u^* v_x^* + v^* v_y^* = -\frac{1}{\rho} p_y^* + v \left( 1 + \frac{1}{\beta} \right) (v_{xx}^* + v_{yy}^*) - \frac{v}{K} v^* + \frac{1}{\rho} \sigma B_0^2 (u^* \sin \gamma \cos \gamma - v^* \cos^2 \gamma) + g \beta_T (T - T_c) + \beta_c (C - C_c) \quad (3)$$

$$u^* T_x^* + v^* T_y^* = \alpha_e (T_{xx}^* + T_{yy}^*) \quad (\text{Fluid region}) \quad (4)$$

$$0 = (T_{xx}^* + T_{yy}^*) \quad (\text{Solid region}) \quad (5)$$

$$u^* c_x^* + v^* c_v^* = D(c_{\mathcal{X}}^* + c_{\mathcal{V}}^*) \quad (6)$$

Where the fluid velocity and temperature are represented by  $\mathbf{u} = (u^*, v^*)$ ,  $T^*$ , and  $p^*$  being the pressure of fluid, respectively.  $\rho$  is the density and  $\sigma$  represents electrical conductivity,  $\alpha$  being the thermal diffusivity of fluid and  $\nu$  indicates the kinematic viscosity. The yield stress,  $\tau_0^*$ , is mathematically expressed as  $\tau_0^* = \frac{\mu^*}{\beta}$ , where  $\beta$  is the parameter of the Casson fluid represents the upper limit of the plastic viscosity. Thermal expansion coefficient is represented by  $\beta$  and magnetic field strength density as  $B_0$  respectively. The dimensionless parameters induced in the problem are  $Ra$ ,  $Pr$  and  $Ha$ ,  $Da$  and  $Le$  numbers.

$$\begin{aligned} \bar{x} = \frac{x}{L}, \bar{y} = \frac{y}{L}, u = \frac{u^*}{\alpha} L, v = \frac{v^*}{\alpha} L, P = \frac{p^* L^2}{\rho \alpha^2}, \theta = \frac{T^* - T_c}{T_h - T_c}, c = \frac{c^* - c_c}{c_h - c_c}, \\ Pr = \frac{\nu}{\alpha_e} R_k = \frac{k_f}{k_s}, \alpha_e = \frac{k_e}{(\rho c_p)_f}, Ra = \frac{\rho \beta_T g L^3 \Delta T Pr}{\nu^2}, Ra_c = \frac{\rho \beta_T g L^3 \Delta c Pr}{\nu^2}, \\ Da = \frac{\kappa}{L^2}, N = \frac{Ra_c}{Ra}, Le = \frac{\alpha_e}{D}, Ha = B_0 L \sqrt{\frac{\sigma}{\mu}} \end{aligned} \quad (7)$$

Using the above dimensionless variables, Eqs. (1) – (6) reduced to

$$u_{\bar{x}} + v_{\bar{y}} = 0 \quad (8)$$

$$\begin{aligned} u u_{\bar{x}} + v u_{\bar{y}} = -p_{\bar{x}} + Pr \left( 1 + \frac{1}{\beta} \right) (u_{\bar{x}\bar{x}} + u_{\bar{y}\bar{y}}) - \frac{Pr}{Da} u \\ + Pr Ha^2 (v \sin \gamma \cos \gamma - u \sin^2 \gamma) \end{aligned} \quad (9)$$

$$\begin{aligned} u v_{\bar{x}} + v v_{\bar{y}} = -p_{\bar{y}} + \nu \left( 1 + \frac{1}{\beta} \right) (v_{\bar{x}\bar{x}} + v_{\bar{y}\bar{y}}) - \frac{Pr}{Da} v \\ + Pr Ha^2 (u \sin \gamma \cos \gamma - v \cos^2 \gamma) + Ra Pr (\theta + Nc) \end{aligned} \quad (10)$$

$$u \theta_{\bar{x}} + v \theta_{\bar{y}} = (\theta_{\bar{x}\bar{x}} + \theta_{\bar{y}\bar{y}}) \quad (11)$$

$$u c_{\bar{x}} + v c_{\bar{y}} = \frac{1}{Le} (c_{\bar{x}\bar{x}} + c_{\bar{y}\bar{y}}) \quad (12)$$

The boundary conditions that are provided take three different forms: hydrodynamics, thermal considerations, and concentration. The other form also includes the remaining cavity walls, which are described by equations (13) to (19)

The surfaces of the fins and the walls enclosing the area have been carefully assessed to have negligible velocity components.



$$u = v = 0 \quad (\text{hydrodynamic boundary condition}) \quad (13)$$

The fins' thermal boundary conditions are expressed in a way that

$$\theta = 0 \quad (\text{left and right cavity walls}) \quad (14)$$

$$\theta = 1 \quad (\text{all circular cylinders}) \quad (15)$$

The following concentration boundary conditions apply to the fin boundaries:

$$c = 0 \quad (\text{left and right cavity walls}) \quad (16)$$

$$c = 1 \quad (\text{all circular cylinders}) \quad (17)$$

$$\frac{\partial \theta_f}{\partial n} = R_k \frac{\partial \theta_{\text{solid}}}{\partial n} \quad (\text{Solid and liquid interface}) \quad (18)$$

The hollow space's remaining boundaries are expressed as such:

$$\theta_n = c_n = 0 \quad (\text{remaining walls of the cavity}) \quad (19)$$

Equations (20) through (24) define the physical parameters of the models, which include the Nusselt number, Sherwood number, Mean Nusselt number, Mean Sherwood number, and total kinetic energy.

$$Nu = \sqrt{\left(\frac{\partial \theta}{\partial x}\right)^2 + \left(\frac{\partial \theta}{\partial y}\right)^2} \quad (\text{Nusselt number}) \quad (20)$$

$$Sh = \sqrt{\left(\frac{\partial c}{\partial x}\right)^2 + \left(\frac{\partial c}{\partial y}\right)^2} \quad (\text{Sherwood number}) \quad (21)$$

$$Nu_{\text{avg}} = \int_{\zeta} Nu \partial \zeta \quad (\text{Mean Nusselt number}) \quad (22)$$

$$Sh_{\text{avg}} = \int_{\zeta} Sh \partial \zeta \quad (\text{Sherwood number}) \quad (23)$$

$$K.E = \frac{1}{2} \int_{\zeta} \|U\|^2 \partial \zeta \quad (\text{Total Kinetic energy}) \quad (24)$$

Entropy generation analysis is a useful tool for estimating the irreversibility or inefficiency of a thermodynamic process. It can provide important information about energy losses and help with system design optimisation. In the case of a fin problem involving a Casson fluid, the analysis is particularly complex because of the fluid's non-Newtonian properties. Within the framework of our particular issue, the total entropy is a combination of contributions from the magnetic field,



heat, friction, and deformation. The entropy generation equations' dimensionless expressions are exemplified by equations (25) through (29).

$$S_{HT} = [(\theta_x)^2 + (\theta_y)^2], \quad (\text{heat transfer}) \quad (25)$$

$$S_{FF} = \phi_1 \left(1 + \frac{1}{\beta}\right) [2(U_x)^2 + 2(V_y)^2 + (V_{xx} + V_{yy})^2], \quad (\text{Fluid friction}) \quad (26)$$

$$S_{DC} = \phi_2 [(C_x)^2 + (C_y)^2] + \phi_3 [(\theta_x C_x + \theta_y C_y)], \quad (\text{Deformation}) \quad (27)$$

$$S_{MF} = \phi_1 Ha^2 (U \sin \gamma - V \cos \gamma)^2, \quad (\text{Magnetic field}) \quad (28)$$

$$S_T = S_{HT} + S_{FF} + S_{DC} + S_{MF}, \quad (\text{Total entropy}) \quad (29)$$

$\phi_1, \phi_2$  and  $\phi_3$  The entropy generation ratio is a common notation for dimensionless quantities, which are usually handled as constants.

The Bejan number, which is a measure of the relative importance of convective and conductive heat transfer in a system, is represented in the model by Equation (30).

$$Be = \frac{S_{HT} + S_{DC}}{S_T} \quad (\text{Bejan number}) \quad (30)$$

### 3. Solution methodology and grid study

The mathematical expression of fluid flow using the Navier-Stokes equations and heat transfer equations is translated into a set of PDEs within **COMSOL Multiphysics v6.0**. This commercially available software employs the finite element method. The computational domain is divided into a finite number of subdomains. Solutions for governing PDEs are obtained at these subdomains by setting a specific convergence criterion. Then after, all solutions are combined by applying the superposition principle. In the current study, iterations are performed for each variable satisfying the stopping criterion  $\left| \frac{\xi^{n+1} - \xi^n}{\xi^n} \right| \leq 10^{-6}$ , where  $\xi$  generally stands for velocity, pressure, temperature and concentration.

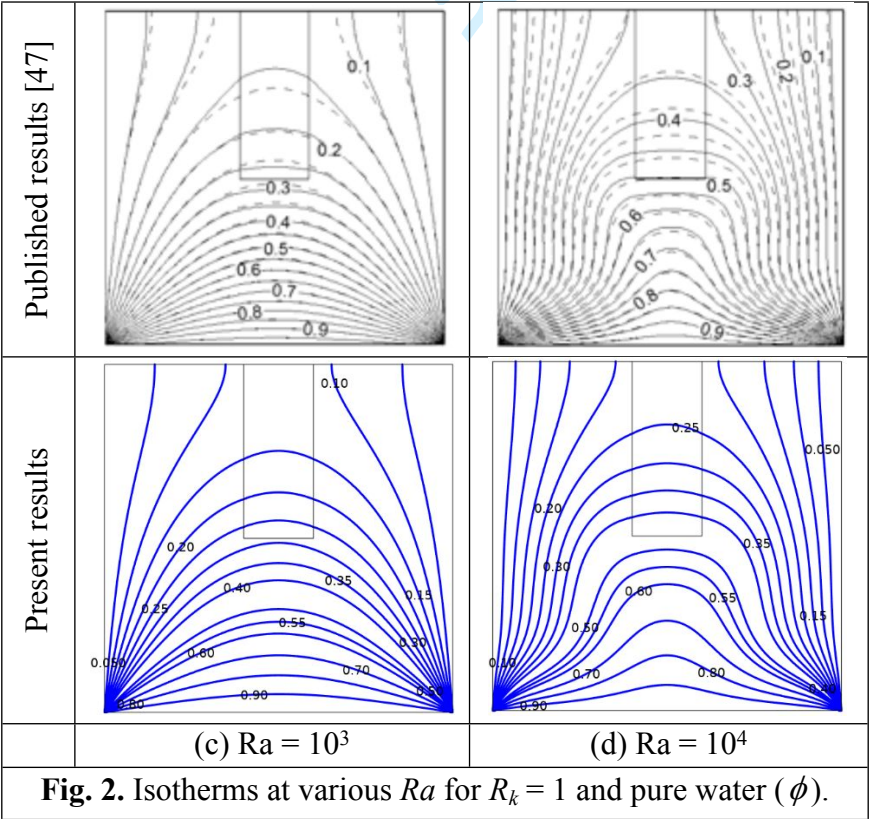
An assessment of mesh independence is performed on a square cavity, and detailed information is provided in Table 1. A grid sensitivity analysis is conducted with consideration of six different element counts: 2618, 4142, 6428, 11080, 15218, and 22824. Results at level 5 and 6 are almost similar even having a big difference in number of elements, hence, for low cost and better results level 5 is the best choice for grid sensitivity study. Therefore, the same grid size is adopted for the rest of computations.

**Table 1.** The average values of Sherwood and Nusselt number at varies elements level.

S.no	#Elements	#Dof	$Nu_{avg}$	$Sh_{avg}$
1	2618	31540	6.4838	8.7703
2	4142	49710	6.7308	9.0618
3	6428	76890	6.8216	9.1701
4	11080	125860	6.8479	9.201
5	15218	171790	6.8713	9.2289
6	22824	247850	6.8726	9.2304

4. Code validation

To validate the present approach, the published findings of Kolsi, L. [47] are employed as a benchmark. The second row of Figure 2 illustrates the variation of isotherms with Ra for the numerical study [47]. The corresponding information for the present study is presented in the second row. **Fig. 3** displays the outcomes from the validation process of the technique for local Nusselt number. These results were juxtaposed against the findings of Kolsi, L. [47]. The acquired values exhibit a satisfactory level of concurrence with those reported by [47].



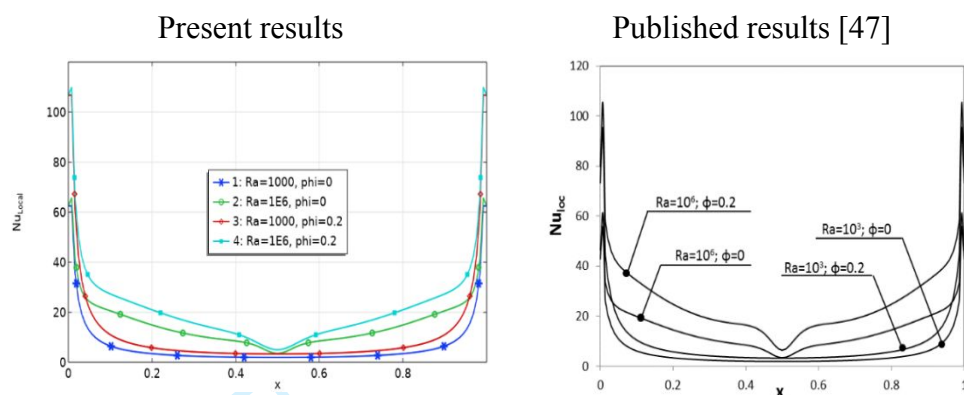


**Fig. 3.** Local Nusselt number at different values of  $Ra$  and  $\phi = 0$  for  $Rc = 1$ .

## 5. Results and discussions

### Case A

In this study, a numerical analysis is executed, and the outcomes are visually represented using isotherms and streamlines. The section provides insights into the variation in local and average  $Nu$ ,  $Sh$ , and entropy production across varying Casson parameters ( $\beta$ ), Rayleigh number ( $Ra$ ), thermal conductivity ratio ( $R_k$ ), Lewis number ( $Le$ ), and Hartmann number ( $Ha$ ). It is to be noted that wherever there is no description of the parameters values then it will be considered as:  $AR = 0.5$ ,  $Ha = 20$ ,  $Pr = 6.2$ ,  $Ra = 10^5$ ,  $Le = 2$ ,  $N = 5$ ,  $R_k = 0.1$ ,  $\gamma = \pi/2$ ,  $Da = 10^{-4}$  and  $\beta = 1$ .

$AR$	Streamlines	Isotherms	Isoconcentrations
------	-------------	-----------	-------------------

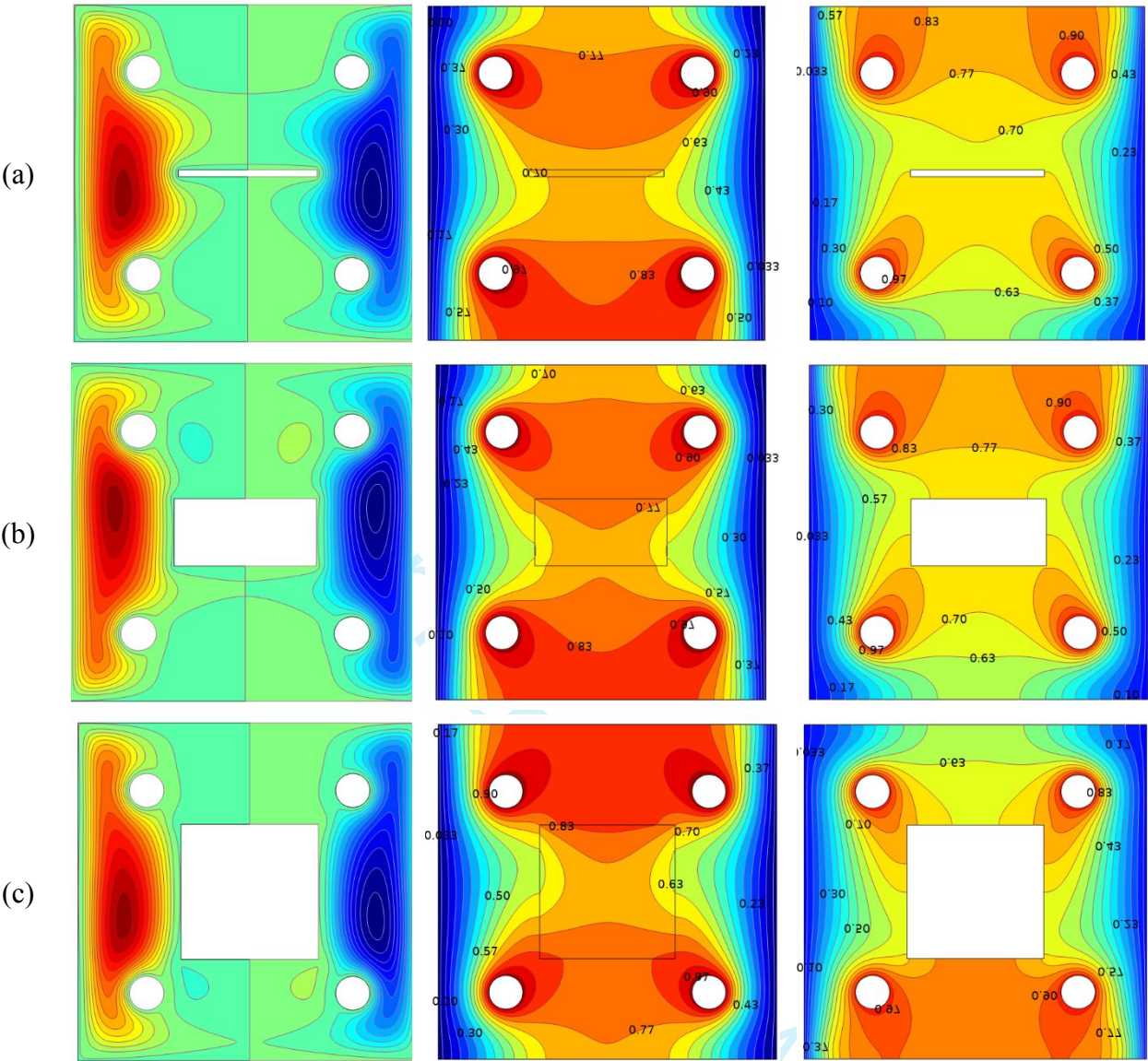
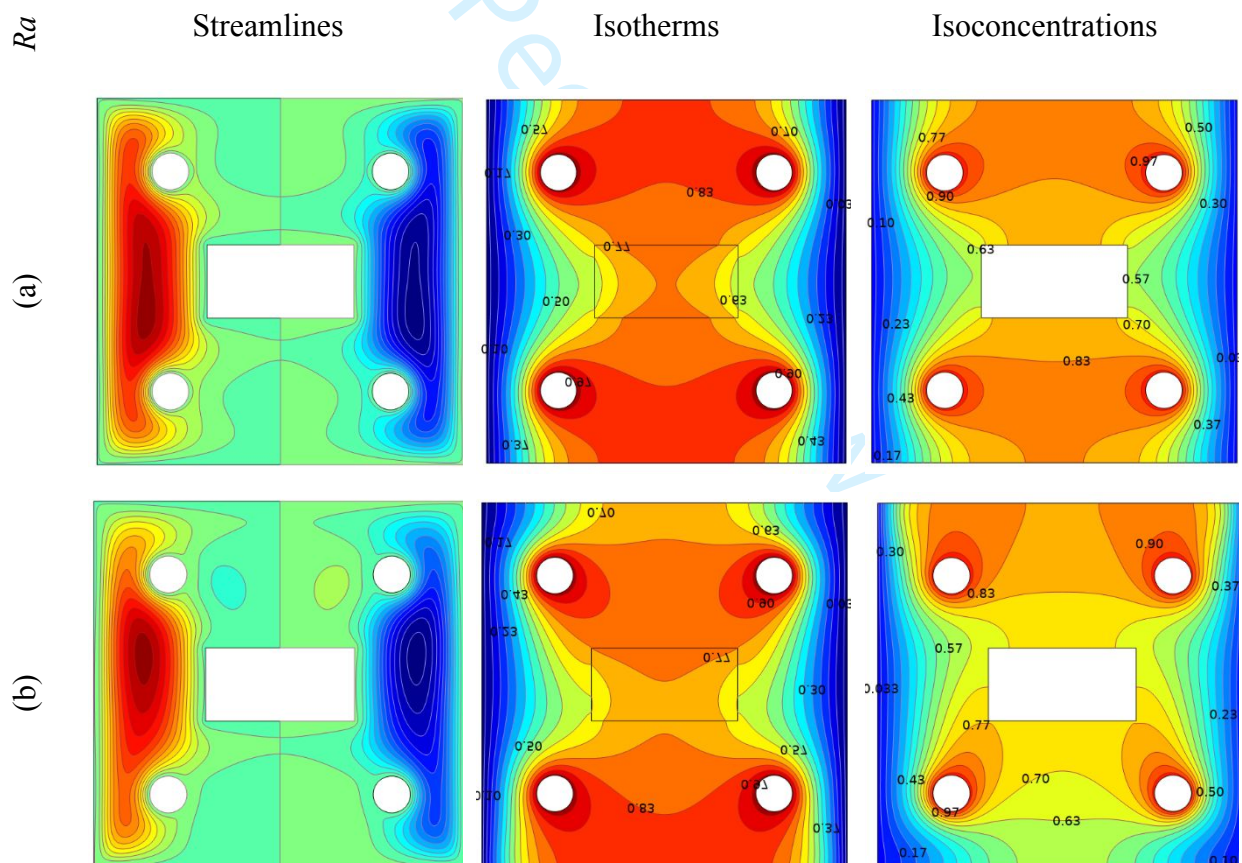


**Fig. 4.** Effects of  $AR$  on streamlines, isotherms and isoconcentrations (a) 0.05, (b) 0.5 and (c) 1.

**Figure 4** shows variations across different values of the parameters and the effect of aspects ratio on streamlines, isotherms, and iso concentration contours. The study includes three aspects ratio ( $AR=0.05, 0.5$  and  $1$ ) and provides a thorough investigation of the influences that each one has on the system’s fluid dynamics, temperature distribution, and concentration gradients. The streamlines show an important pattern for a given aspect ratio  $AR=0.05$ , with the strength of circulations getting more prominent in cases with smaller aspect ratios than in cases with higher  $AR$  values. A consistent finding appears across the aspect ratio range, indicating the formation of two main circulation cells inside the enclosure. It is noteworthy, though, that small secondary cells can be seen forming around the heated circular obstacle at higher  $AR$  values. This phenomenon



suggests that aspect ratio has a discernible impact on the circulation patterns inside the enclosure, with higher values of AR exhibiting additional circulation features and lower values favoring stronger circulation. Convection is the predominant process throughout the entire range of AR values, as indicated by the isothermal lines shown in **Figure 4** (a, b and c). Specifically, when AR takes smaller values, the heat transfer around the rectangular obstacle that lies between gets more prominent. On the other hand, closer to the heated circular cylinders next to the wall, as AR rises, the isothermal lines show concentration, signifying increased heat transfer rates. When the aspect ratio is reduced, the iso-concentration lines distance themselves from the boundaries by lining up nearly parallel in the middle of the enclosure. The influence of thermal buoyancy increases with the rectangular block's aspect ratio (AR), particularly for the values of  $N$  greater than 1. The concentration contours become distorted as this phenomenon becomes more significant. As a result, these shapes depart from the middle and eventually arrive at the hot cylinders.



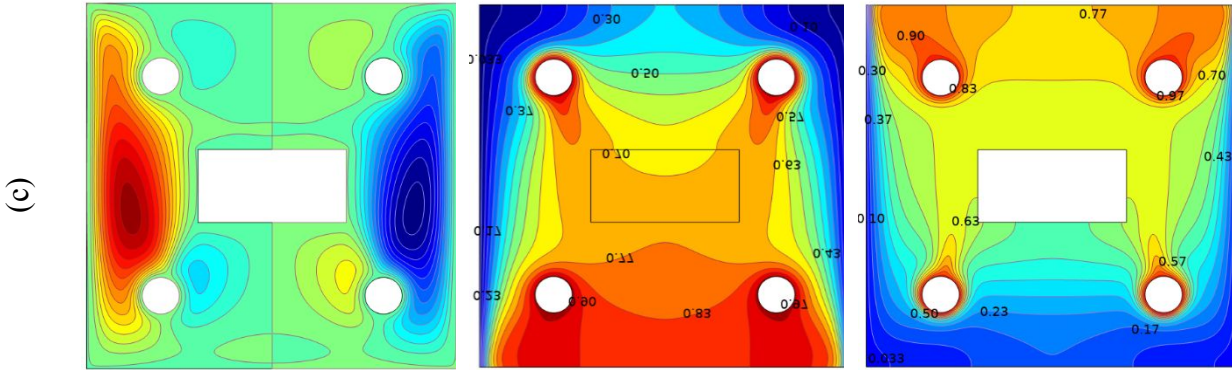


**Fig. 5.** Effects of  $Ra$  on streamlines, isotherms and iso contractions (a) $10^4$ , (b) $10^5$  and (c) $10^6$ .

The effects of the Rayleigh number on streamlines, isotherm, and iso concentration patterns at given parameter setting are illustrated graphically in **Figure 5**. The Rayleigh number has a major influence in the dynamics of natural convection phenomena. Natural convection occurs when temperature fluctuates occurs in a fluid medium because they cause changes in density. A rising flow driven by buoyancy forces results from the fluid's decreasing density as temperature rises, at a Rayleigh number ( $Ra$ ) of  $10^4$ , viscous forces are more common than buoyant and Lorentz forces, which prevents the flow from starting. One interesting finding is that the fluid around the circular cylinder heats up and moves towards the colder rectangular block. Rising along the circular cylinders, resulting in the creation of recirculation zones. High Rayleigh numbers ( $Ra$ ) cause a discernible suppression of convection in the vicinity of insulated boundaries. At  $Ra=10^4$ , circulation cells are dispersed equally throughout the enclosures. A further increase in the Rayleigh number to  $Ra=10^5$  causes the circulation cells to concentrate near the bottom of the enclosure. This concentration is explained by increased convective effects resulting from increased buoyant forces. The impact of the Rayleigh number on the rate of heat transfer is made evident by looking at the iso thermal contours in **Figure 5** (a, b and c).

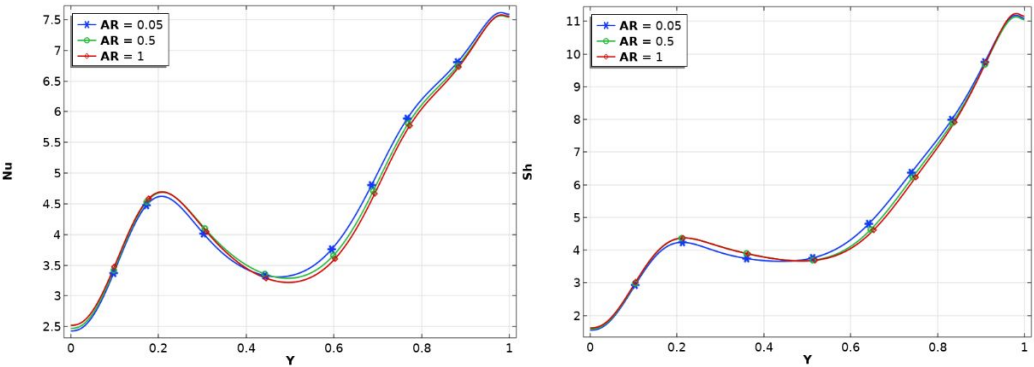


**Figure 6.** Effects of  $AR$  on Local Nusselt number and Sherwood number.

**Figure 6** illustrate that the effect of an increasing aspect ratio on the local Nusselt number and Sherwood numbers, respectively, for the given parameter values. The local heat and mass transfer rates are higher near the heated cylinders and then decreases. The graph individually clearly show a rising  $AR$  in conjunction with an elevated trend of Sherwood and Nusselt numbers. The observation phenomenon can be explained by the dominant convective effects inside the enclosure, which become more pronounced as the aspect ratio increases

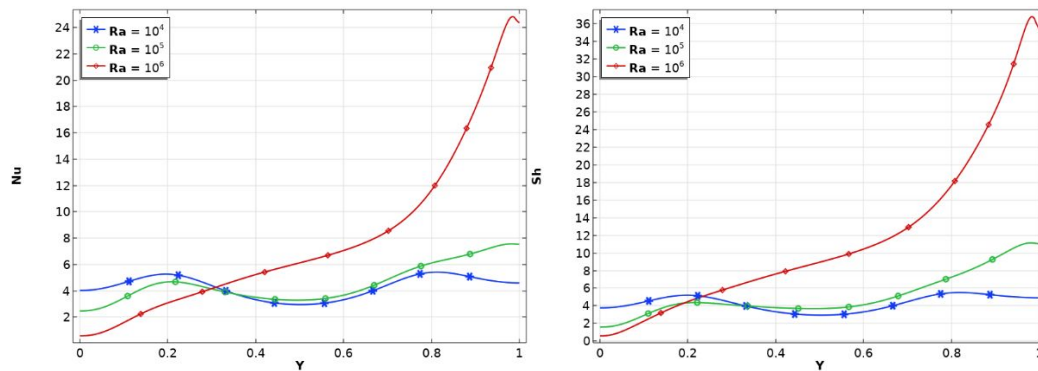


**Fig 7.** Effects of  $Ra$  on Local Nusselt number and Sherwood number.

**Figure 7** illustrate the effect of an increasing Lewis number for the given parameter values for the local Nusselt and Sherwood numbers, respectively, Plots of the individual numbers clearly show a trend whereby raising the Lewis number leads to higher Nusselt and Sherwood numbers. The dominant convective forces in the enclosure, which become more pronounced as Lewis' number increases, can be used to explain this behavior.

Shape optimaization in term of aspect ration has been investigated in Table 2 and 3. The  $AR$  is varied and different types of entropies are calculated as reported in Table 2. It is observed that all types of entropy intensify as  $AR$  increases. This is due to more turbulence in the flow. Secondray vortex formation can be seen at higher  $AR$ . The  $Be$  changes from 0.1076 to 0.1322 as we changed  $AR$  from 0.05 to 1. Insignificant decrease in  $Nu_{avg}$  of 1.13% is calculated for the considered value of  $AR$  (see Table 3). This minor impact is due conductive behavior of the block.

**Table 2.** Aspect ratio impact on entropies and Bejan number.

$AR$	$S_{HT}$	$S_{FF}$	$S_{DC}$	$S_{MF}$	$S_T$	$Be$
0.05	9.5403	148.94	6.2188	0.49927	165.20	0.1076
0.2	9.7759	149.29	6.3700	0.48385	165.92	0.1123
0.4	10.099	150.73	6.5808	0.46848	167.88	0.1176
0.6	10.436	153.27	6.8048	0.46068	170.98	0.1227



0.8	10.795	157.03	7.0470	0.45985	175.33	0.1282
1	11.186	161.99	7.3125	0.46019	180.95	0.1322

**Table 3.** Variations in mean heat and mass transfer rates with varying Aspect ratio.

<i>AR</i>	<i>Nu<sub>avg</sub></i>	<i>Sh<sub>avg</sub></i>	<i>K.E<sub>avg</sub></i>
0.05	4.5832	5.1763	33.586
0.2	4.5795	5.1684	33.618
0.4	4.5699	5.1567	33.883
0.6	4.5571	5.1446	34.401
0.8	4.5435	5.1345	35.188
1	4.5313	5.1281	36.2

**Table 4** examines the influence of Rayleigh number (*Ra*) on entropy generation resulting from the combined action of fluid friction, magnetic field force, and heat transfer. The study also explores the effect is increasing *Ra* values on the  $S_{HT}$ ,  $S_{FF}$ ,  $S_{DC}$ ,  $S_{MF}$ ,  $S_T$  and  $Be$  from  $10^3$  to  $10^6$ . The magnitude of total entropy generation abruptly increases. Increasing the obstacle’s aspects ratio can improve flow restriction inside a cavity and cause changes to flow patterns and velocity distributions. One of the most important factors affecting the total surface area allotted to heat transfer in a rectangular obstacle is its aspects ratio. As a result, this enhancement greatly increases the heat transfer between the rectangular barrier and the surrounding fluid, resulting in elevated convective heat transfer rates. Because of the contributions of both  $S_{FF}$  and  $S_{HT}$ , this makes  $S_T$  more valuable. With an increase of *Ra* in the considered range, the *Be* was changed from 0.976 to 0.0134.

**Table 4.** Effects of *Ra* on entropies.

<i>Ra</i>	$S_{HT}$	$S_{FF}$	$S_{DC}$	$S_{MF}$	$S_T$	<i>Be</i>
$10^3$	9.6575	0.01707	5.7929	6.85E-05	15.467	0.976
$10^4$	9.666	1.7052	5.8084	0.0068036	17.186	0.66851
$10^5$	10.265	151.86	6.6909	0.4636	169.28	0.11999
$10^6$	17.548	5582.9	13.876	10.183	5624.5	0.0134

**Table 5** shows, for the given parameter values, how Rayleigh number ( $Ra$ ) affects  $Nu_{avg}$ ,  $Sh_{avg}$ ,  $K.E_{avg}$  and heat transfer inside an enclosure. A higher Rayleigh number of an observations cause flow restriction inside the cavity when  $Ra$  rises. Change in the distribution of velocity and flow pattern follow. The total surface area available for heat transfer is directly influenced by the rectangular obstacle's Rayleigh number, which results in increased convective heat transfer rates between the obstacle and the surrounding fluid. When  $Ra$  was changed from  $10^3$  to  $10^6$  the change in  $Nu_{avg}$ ,  $Sh_{avg}$  and  $K.E_{avg}$  was reported from 4.2971, 4.2896 and .0039 to 7.7988, 11.518 and 1168.9, respectively.

Table 5. Effects of  $Ra$  on mean values.

$Ra$	$Nu_{avg}$	$Sh_{avg}$	$K.E_{avg}$
$10^3$	4.2971	4.2896	0.0039
$10^4$	4.3008	4.3048	0.38591
$10^5$	4.5638	5.1506	34.109
$10^6$	7.7988	11.518	1168.9

Table 6 examines how the combine effects of fluid friction, magnetic field force, and heat transfer affect the generation of entropy as a function of Hartmann number ( $Ha$ ). The impact of rising  $Ha$  values on the  $S_{HT}$ ,  $S_{FF}$ ,  $S_{DC}$ ,  $S_{MF}$ ,  $S_T$  and  $Be$  from 0 to 100. The generation of total entropy is strongly increased. A cavity's flow restriction is increased when obstacles have an aspect ratio greater than one, which changes flow patterns and velocity distributions. One of the most important factors affecting the overall surface area allotted to heat transfer in a rectangular obstacle is its aspect ratio. As a result, this improvement significantly increases convective heat transfer rates by boosting heat transfer between the surrounding fluid and the rectangular barrier.

**Table 6.** Effects of  $Ha$  on entropies.

$Ha$	$S_{HT}$	$S_{FF}$	$S_{DC}$	$S_{MF}$	$S_T$	$Be$
0	10.272	153.15	6.6998	0	170.13	0.11952
25	10.261	151.14	6.686	0.71695	168.81	0.12026
50	10.229	145.5	6.6475	2.6436	165.02	0.12271
75	10.183	137.14	6.5914	5.2729	159.19	0.12763

100	10.132	127.1	6.5256	8.1075	151.86	0.13648
-----	--------	-------	--------	--------	--------	---------

**Table 7** shows how  $Ha$  affect  $Nu_{avg}$ ,  $Sh_{avg}$ ,  $K.E_{avg}$  and heat transfer in an enclosure for the given parameter value. A higher Hartmann number can improve the cavity’s flow restriction, which will affect the distribution of flow and velocity. An increase in the Hartmann number modifies the total surface area allotted to heat transfer. This improvement therefore encourages convective heat transfer rates between the surrounding fluid and rectangular obstacle. Jan and Farooq [48, 49] found similar results with effects of magnetic parameters on velocity and heat flow.

**Table 7.** Effects of  $Ha$  on mean values.

$Ha$	$Nu_{avg}$	$Sh_{avg}$	$K.E_{avg}$
0	4.5671	5.1588	34.408
25	4.562	5.146	33.943
50	4.5479	5.1104	32.64
75	4.5279	5.0582	30.713
100	4.5052	4.9966	28.403

**Case B**

In this study, a numerical analysis is executed, and the outcomes are visually represented using isotherms and streamlines. The section provides insights into the variation in local and average  $Nu$ ,  $Sh$ , and entropy production across varying Casson parameters ( $\beta$ ), Rayleigh number ( $Ra$ ), Lewis number ( $Le$ ), and Hartmann number ( $Ha$ ). It is to be noted that wherever there is no description of the parameters values then it will be considered as:  $AR = 0.5$ ,  $Ha = 20$ ,  $Pr = 6.2$ ,  $Ra = 10^5$ ,  $Le = 2$ ,  $N = 5$ ,  $\gamma = \pi/2$ ,  $Da = 10^{-4}$  and  $\beta = 1$ .

$R$

Streamlines

Isotherms

Isoconcentrations

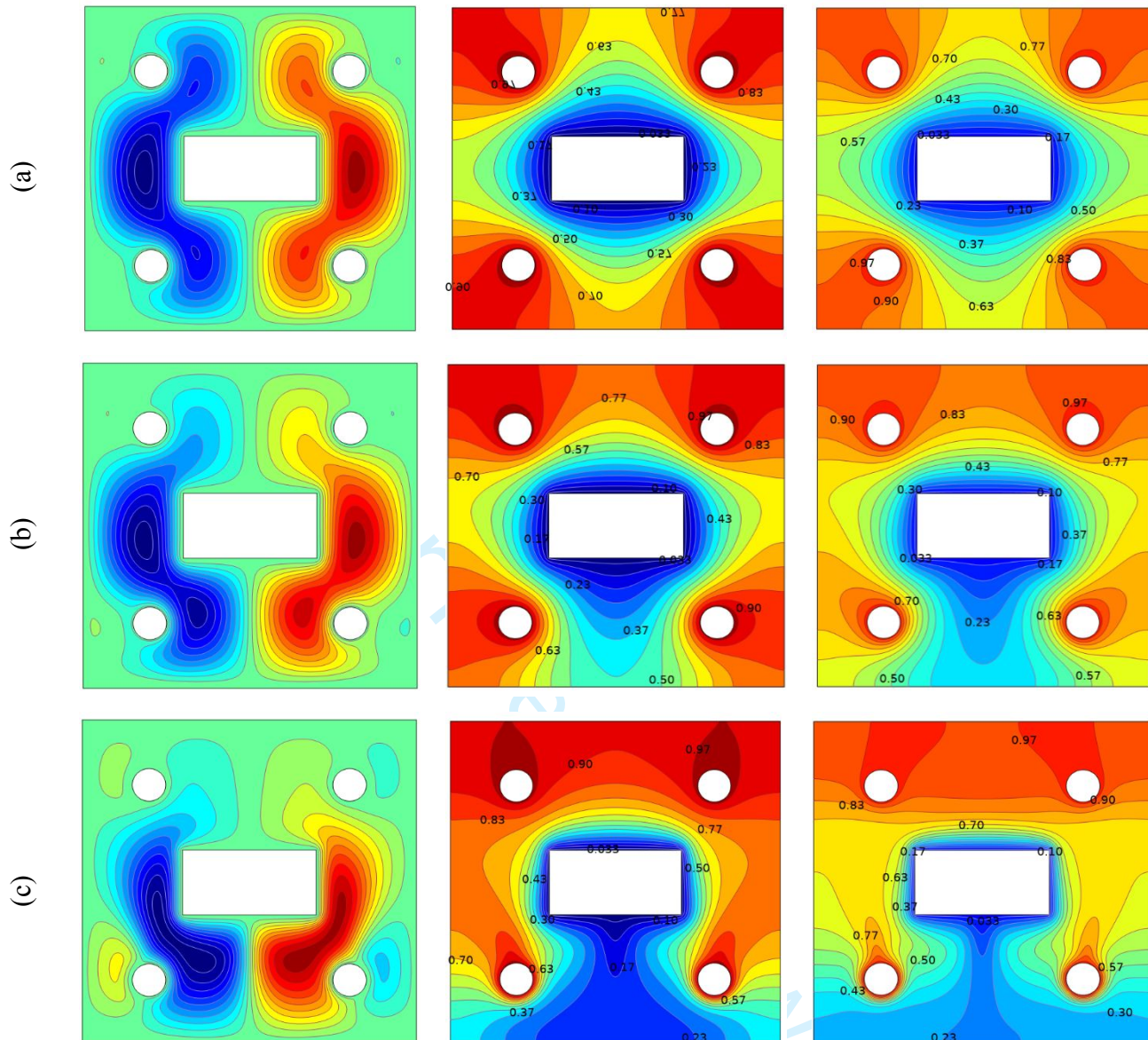


**Fig. 8.** Effects of  $Ra$  on streamlines, isotherms and isoconcentrations (a) $10^4$ , (b) $10^5$  and (c) $10^6$ .

The effects of the Rayleigh number on streamlines, isotherm, and iso concentration patterns at given parameter setting are illustrated graphically in **Figure 8**. The Rayleigh number has a major influence in the dynamics of natural convection phenomena. Natural convection occurs when temperature fluctuates in a fluid medium because they cause changes in density. A rising flow driven by buoyancy forces results from the fluid's decreasing density as temperature rises, at a Rayleigh number ( $Ra$ ) of  $10^4$ , viscous forces are more common than buoyant and Lorentz forces, which prevents the flow from starting. One interesting finding is that the fluid around the circular



cylinder heats up and moves towards the colder rectangular block. Rising along the circular cylinders, resulting in the creation of recirculation zones. High Rayleigh numbers ( $Ra$ ) cause a discernible suppression of convection in the vicinity of insulated boundaries. At  $Ra=10^4$ , circulation cells are dispersed equally throughout the enclosures. A further increase in the Rayleigh number to  $Ra=10^5$  causes the circulation cells to concentrate near the bottom of the enclosure. This concentration is explained by increased convective effects resulting from increased buoyant forces. The impact of the Rayleigh number on the rate of heat transfer is made evident by looking at the iso thermal contours in **Figure 7** (a, b and c).

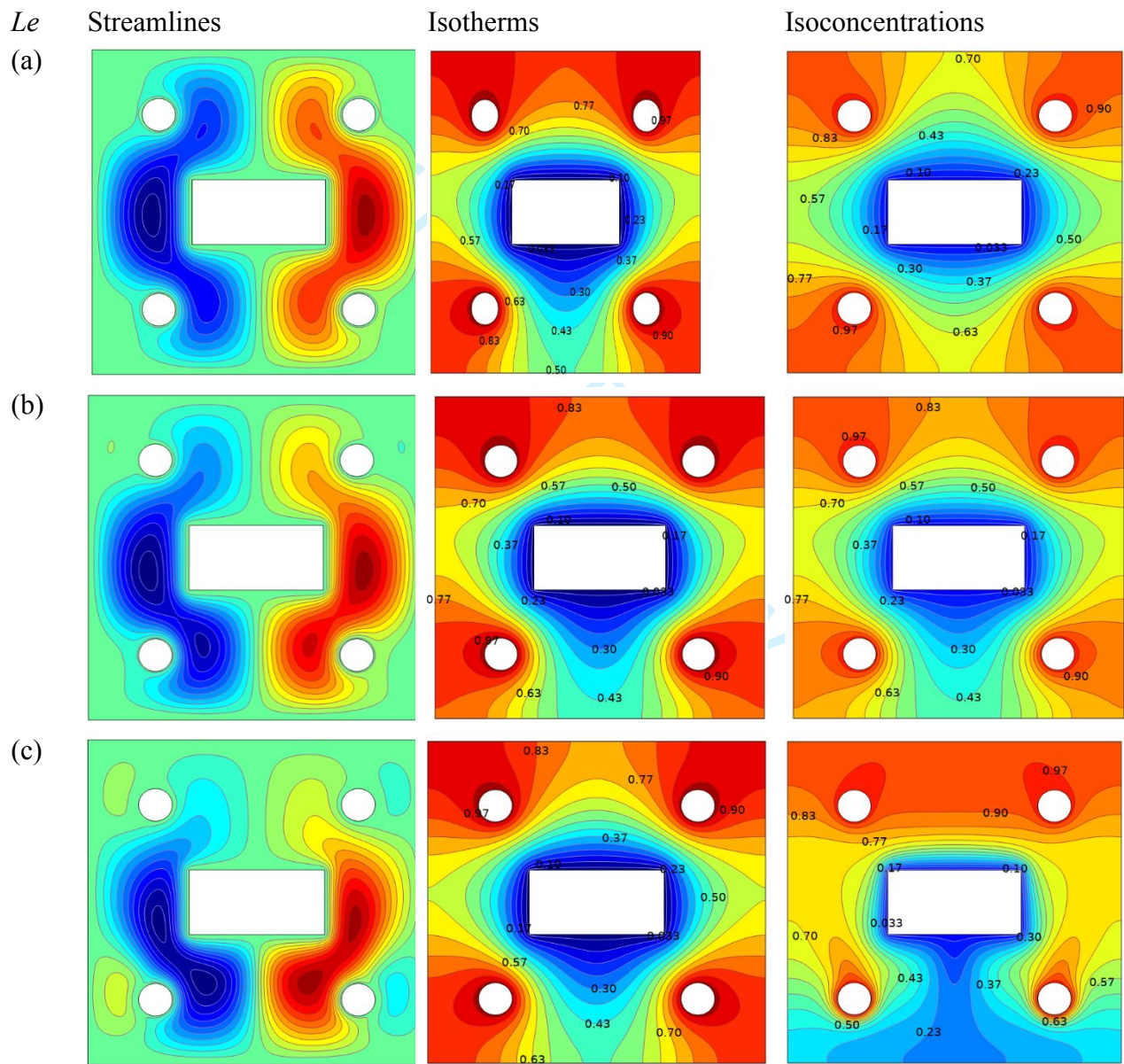


**Fig. 9.** Effects of  $Le$  on streamlines, isotherms and iso-concentrations (a)0.01, (b)1 and (c)10.

**Figure 9** Shows how the Lewis number effects streamline, isotherm, and iso-concentration contour features in a fluid-filled enclosure. The changes in streamlines are displayed in the first column on the left. Interestingly, when the Lewis number ( $Le$ ) is adjusted to 0.01, two prominent cells exhibit a clear symmetric configuration that essentially encloses the cavity. On the other hand, cells formed inside the cavity are noticeably weaker when the  $Le$  values are equal to 1, and their concentration is primarily in the lower part of the enclosure. On the other hand, cells form inside the cavity are noticeable weaker when the value of  $Le=1$ , and their concentration is primarily in the lower part of the enclosure. A greater number of cells from throughout the enclosure and a slight decrease in overall flow strength occur as the value of  $Le$  rises. The middle column of the **Figure 9** shows the distribution of isotherms for various  $Le$  values. The isotherms show a density packed arrangement closes to the Cavity's center zone for lower  $Le$  values. The strong conduction mechanism that predominates in that particular area is responsible for this observed pattern. When the  $Le$  values increase, the isotherms in the middle deform, indicating the formation of the convective zone. As  $Le$  values rise one after another, the isothermal contours gradually enclose the entire enclosure. The iso-concentration contours are dispersed uniformly throughout the cavity at  $Le=0.01$ . on the other hand, for high  $Le$  vales, these contours show a tendency towards concentration near the enclosure's rectangle block and lower circular cylinder, with a noticeable distortion near the outer boundary.

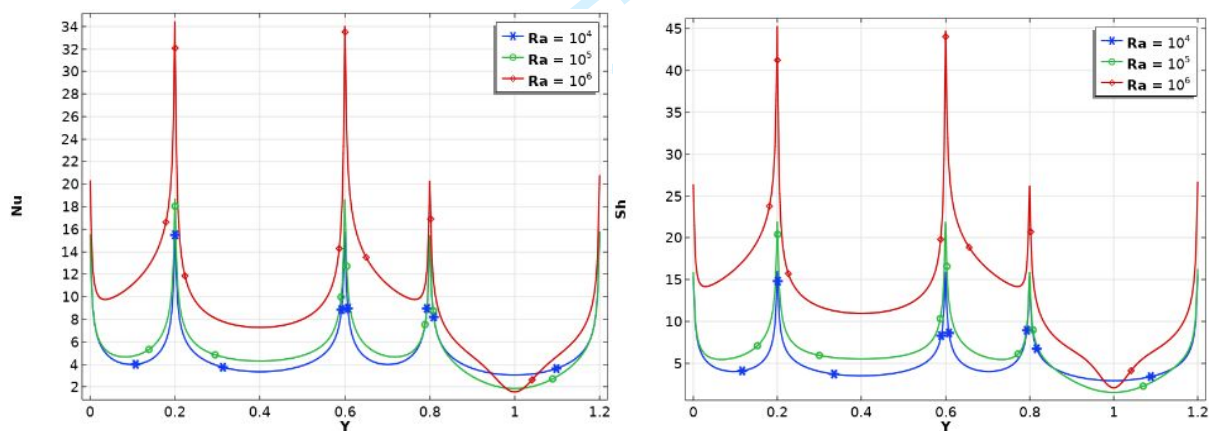


**Fig 10.** Effects of  $Ra$  on Local Nusselt number and Sherwood number.

**Figure 10** Shows the effect of an increasing Rayleigh number on the local Nusselt and Sherwood numbers, respectively, for the given parameter values. The lone graphs show a clear pattern that increases Nusselt and Sherwood numbers as the Rayleigh number rises. This phenomenon can be explained by the dominant convective effects inside the enclosure, which become more pronounced as the Rayleigh number rises.

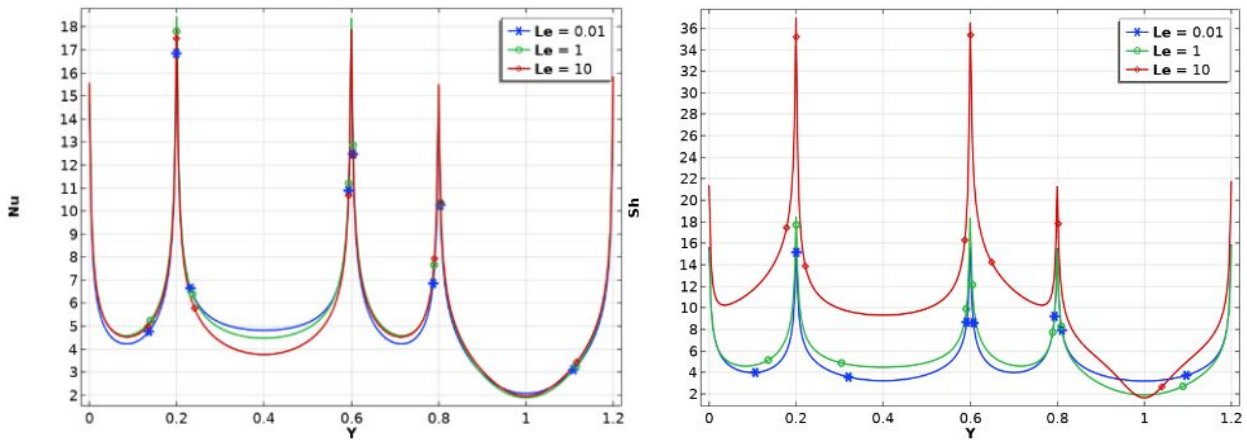


**Fig 11.** Effects of  $Le$  on Local Nusselt number and Sherwood number.

Figure 11 illustrate the effect of an increasing Lawis number for the given parameter values for the local Nusselt and Sherwood numbers, respectively, Plots of the individual numbers clearly show a trend whereby raising the Lewis number leads to higher Nusselt and Sherwood numbers. The dominant convective forces in the enclosure, which become more pronounced as Lewis' number increases, can be used to explain this behavior.

**Table 8** examines the influence of Rayleigh number on entropy generation resulting from the combined action of fluid friction, magnetic field force, and heat transfer. The study also explores the effect id increasing  $Ra$  values on the  $S_{HT}$ ,  $S_{FF}$ ,  $S_{DC}$ ,  $S_{MF}$ ,  $S_T$  and  $Be$  from  $10^3$  to  $10^6$ . The magnitude of total entropy generation abruptly increases. Increasing the obstacle's aspects ratio can improve flow restriction inside a cavity and cause changes to flow patterns and velocity distributions. One of the most important factors affecting the total surface area allotted to heat transfer in a rectangular obstacle is its aspects ratio. As a result, this enhancement greatly increases the heat transfer between the rectangular barrier and the surrounding fluid, resulting in elevated convective heat transfer rates. Because of the contributions of both  $S_{FF}$  and  $S_{HT}$ , this makes  $S_T$  more valuable.

**Table 8.** Effects of  $Ra$  on entropies.

$Ra$	$S_{HT}$	$S_{FF}$	$S_{DC}$	$S_{MF}$	$S_T$	$Be$
$10^3$	6.5739	0.0067	3.9444	4.13E-05	10.525	0.9912
$10^4$	6.5783	0.6884	3.9523	0.0042	11.223	0.77951
$10^5$	7.0831	88.505	4.6586	0.5571	100.8	0.1662
$10^6$	12.491	2938.1	9.5592	15.95	2976.1	0.0262

**Table 9** shows how  $Ra$  effect on  $Nu_{avg}$ ,  $Sh_{avg}$ ,  $K.E_{avg}$  and heat transfer in an enclosure for the given parameter value. A higher  $Ra$  can improve the cavity's flow restriction, which will affect the



distribution of flow and velocity. An increase in the  $Ra$  modifies the total surface area allotted to heat transfer. This improvement therefore encourages convective heat transfer rates between the surrounding fluid and rectangular obstacle.

**Table 9.** Effects of  $Ra$  on mean values.

$Ra$	$Nu_{avg}$	$Sh_{avg}$	$K.E_{avg}$
$10^3$	4.7796	4.7797	0.0015
$10^4$	4.7827	4.7923	0.158
$10^5$	5.1483	5.8946	20.298
$10^6$	9.0969	12.873	623.63

**Table 10** examines the joint effects of heat transfer, magnetic field strength, and fluid friction on entropy production as a function of  $Le$ . The investigation examines how increasing  $Le$  values affect a range of parameters from 0.01 to 10, including heat transfer, flow patterns, and velocity distributions. As  $Le$  values rise, there is a noticeable increase in total amount of entropy generated. When obstacles have an aspect ratio larger than one, there is increased flow restriction within the cavity, which causes changes to the flow patterns and velocity distributions. One important factor that affects the total surface area devoted to heat transfer in a rectangular obstacle is its aspect ratio. As a result, by encouraging effective heat exchange between the surrounding fluid and rectangular barrier, this improvement significantly increases convective heat transfer rates.

**Table 10.** Effects of  $Le$  on entropies.

$Le$	$S_{HT}$	$S_{FF}$	$S_{DC}$	$S_{MF}$	$S_T$	$Be$
0.01	6.9745	68.329	3.9455	0.41471	79.664	0.16122
1	7.0785	87.575	4.2471	0.55462	99.456	0.15622
10	6.8439	44.935	6.3841	0.26528	58.428	0.29012

**Table 11** shows, for the given parameters values, how  $Le$  effects on  $Nu_{avg}$ ,  $Sh_{avg}$ ,  $K.E_{avg}$  and flow distribution, velocity, and heat transfer inside an enclosure. The flow restriction of the cavity can be improved with a higher  $Le$  number, which will affect the flow and velocity distribution. An increase in the  $Le$  number causes changes to the total area allotted to heat transfer. This improvement consequently encourages convective heat transfer rates between the surrounding fluid and the rectangular barrier.

**Table 12** explain the variation in the Casson fluid parameter influences on heat transfer, fluid fraction, deformation, magnetic field, total entropy and bejan number various used for the entropy generation of the proposed model. Increase in the casson fluid parameter enhance the heat transfer of the system due to the change in the behaviour of the shear-thinning. The fluid fraction described in the third column of the table get lowered because of the decrease in the quantity of yield stresses. Moreover, the resistance to deformation increases with a higher Casson fluid parameter. The magnetic field effect is explained in the 5<sup>th</sup> column of the table. It is raised with the increase in the value of the Casson fluid parameter due to the increase in the resistive Lorentz forces. The total entropy effect with the variation in Casson fluid parameter is presented in the 2<sup>nd</sup> last column of the table. The total entropy of the system decreases because of the controlled disordered in the system. The effect of Bejan number is depicted in the last column of the table, it is noticed that the its value get higher for the raise in the Casson fluid parameter.

**Table 13** presents the effect of the Casson fluid parameter  $\beta$  on the  $Nu_{avg}$ ,  $Sh_{avg}$ , and average kinetic energy  $K.E_{avg}$ . As  $\beta$  increases, indicating a higher non-Newtonian behavior of the Casson fluid,  $Nu_{avg}$  also increases. This happens due to the decrease in the resistance to the fluid flow. Enhancing the convective heat transfer from the hot circular cylinders to the cooler central rectangular object. Analogous to the Nusselt number, the Sherwood number also increase with the variation in  $\beta$  implies that the mass transfer `rate is also enhanced, due to the same decrease in fluid resistance. The average kinetic decrease with the change in  $\beta$  indicates that the fluid's motion becomes more vigorous, resulting from the reduced viscosity at higher  $\beta$  values, leading to more turbulent flow patterns.

Table 11. Effects of  $Le$  on mean values.

$Le$	$Nu_{avg}$	$Sh_{avg}$	$K.E_{avg}$
0.01	5.0724	4.7796	15.676
1	5.1458	5.1457	20.146
10	4.9731	10.058	9.9089

**Table 12.** Effects of  $\beta$  on entropies.

$\beta$	$S_{HT}$	$S_{FF}$	$S_{DC}$	$S_{MF}$	$S_T$	$Be$
0.1	6.8298	232.31	4.3323	0.2895	243.76	0.097614
1	7.0831	88.505	4.6586	0.5571	100.8	0.1662
5	7.1411	60.284	4.7323	0.6141	72.772	0.2062

10	7.15	56.343	4.7437	0.6227	68.86	0.2140
----	------	--------	--------	--------	-------	--------

**Table 13.** Effects of  $\beta$  on mean values.

$\beta$	$Nu_{avg}$	$Sh_{avg}$	$K.E_{avg}$
0.1	4.9645	5.3923	10.035
1	5.1483	5.8946	20.298
5	5.1903	6.0074	22.604
10	5.1968	6.0249	22.959

The impact of the thermal conduction scenario of the system geometry and the variation of the magnetic field inclination effect on heat transfer, fluid fraction, deformation, magnetic field, total entropy and bejan number is depicted in Table 14 at  $Ha = 100$ . The change in the orientation of the magnetic field potentially alter the efficiency of the heat transfer from hot to cold areas due to the creation of temperature gradients, as well as the alignment of the field lines increase the heat transfer. The change in the angle of magnetic field influence the strength of the Lorentz forces from lower to higher value in the range of  $0^\circ$ - $90^\circ$ . This variation change the flow pattern which leads to higher the fluid fraction and deformation. The strength of the magnetic field is interpreted in the 5<sup>th</sup> column of the table showing decrease in its strength for the variation in its inclination angle from  $0^\circ$  degree to  $90^\circ$ . total entropy of the system decrease as the inclination angle get increase due to the raise in the disorder of the system. The impact on the Bejan number is described in the last column. Which shows that at the lower inclination the energy distribution is more efficient than the higher value of the angle. This results in the decrease of the Bejan number.

Table 15 describe the impact of orientation of the magnetic field on average Nusselt number, average Sherwood Number and average kinetic energy at various values of  $\gamma$  and  $Ha = 100$  while taking other paraters fis as illusted in the first paragraph of case A. The 2nd column of the table demonstrate average Nusselt number which increased as the orientation change from  $0^\circ$ - $90^\circ$ . The rectangular object in the center, which is conductive in case A and isothermal in case B, interacts with the surrounding fluid under the influence of the magnetic field. As  $\gamma$  increases, the magnetic field lines become more perpendicular to the object, potentially enhancing turbulence in the fluid and thereby increasing convective heat transfer. This leads to an increase in average Nusselt number. The numeric value of heat transfer rate shows that as we changed inclination from horizontal to vertical its value changed from 4.9717 to 5.0112. Similarly, the effect on Sherwood

number is explained in the 3rd column which is also increasing due to the enhancement in the quantity of the mass transfer. The mass transfer is influenced by the temperature and concentration differences between the rectangular cylinder and the circular objects, as well as the magnetic field inclination,  $\gamma$ . An increase in  $\gamma$  enhance the convective mass transfer due to increased fluid motion and mixing, leading to an increase in average Sherwood number. The last column of the table study the average kinetic energy of the fluid particles. The motion of these particles is influenced by the magnetic field, the temperature and concentration gradients, and the geometry of the system. As  $\gamma$  increases, the Lorentz force acting on the charged particles in the fluid increases, potentially inducing more vigorous fluid motion and turbulence. This leads to an increase in average kinetic energy.

**Table 14.** Effects of  $\gamma$  on entropies and Bejan number.

$\gamma$	$S_{HT}$	$S_{FF}$	$S_{DC}$	$S_{MF}$	$S_T$	$Be$
0°	6.8410	39.100	4.3554	10.700	60.997	0.22074
45°	6.8714	48.661	4.3986	9.2374	69.168	0.20946
90°	6.8938	58.845	4.4339	7.7077	77.880	0.18658

**Table 15.** Effects of  $\gamma$  on mean Nusselt and Sherwood number and kinetic energy.

$\gamma$	$Nu_{avg}$	$Sh_{avg}$	$K.E_{avg}$
0°	4.9717	5.4285	8.8828
45°	4.9943	5.4970	11.051
90°	5.0112	5.5539	13.368

6. Conclusion

The finding of this study examines a two-dimensional square enclosure embedded with circular squares at the corners and an endothermic rectangular cylinder at the center. In depth investigation of heat transfer, magnetic field effects, and non-Newtonian Casson fluid flow. A no-slip velocity condition, specific temperature and concentration characterize the cavity. Governing equations for mass, momentum, energy, and concentration conservation are applied, considering laminar, incompressible, and steady-state flow with constant fluid properties. The whole manuscript was divided into two sections, case A and case B. In case A, the internal rectangular object was considered conductive with specific conductivity, and cavity walls were kept at a constant lower temperature. In case B, all cavity walls were considered adiabatic and the rectangular block was

set to a lower temperature. The meticulous investigations were made for the flow structure, heat transfer and mass flow. The following are the main points observed during the investigation.

- It was observed that all types of entropy intensified as  $AR$  increased. This is due to more turbulence in the flow and formation of secondary vortices. The  $Be$  changed from 0.1076 to 0.1322 as we changed  $AR$  from 0.05 to 1. An insignificant effect of  $AR$  was seen on  $Nu_{avg}$  and 1.13% decrease was calculated by changing it from 0.05 to 1. All these outcomes have been extracted from case A.
- Higher Rayleigh numbers lead to distinct circulation patterns, recirculation zones, and variations in heat transfer rates within the enclosure. In case A, when  $Ra$  was changed from  $10^3$  to  $10^6$  the change in  $Nu_{avg}$ ,  $Sh_{avg}$  and  $KE_{avg}$  was reported from 4.2971, 4.2896 and .0039 to 7.7988, 11.518 and 1168.9, respectively. At the same time, the  $Be$  was changed from 0.97 to 0.013.
- In case A, the local heat and mass transfer rates are higher near the heated cylinders and then decreases. Increasing in the aspect ratio raise the local Nusselt and Sherwood numbers, showing intensified convective effects within the enclosure.
- The heat loss through the boundary in case B was calculated with the effects of magnetic inclination. The magnetic field give rise to induced magnetic field which results to affect the flow structure. The numeric value of heat transfer rate shows that as we changed inclination from horizontal to vertical its value changed from 4.9717 to 5.0112.
- Increasing Lewis number results in higher local Nusselt and Sherwood number, demonstrate elevated convective forces within the enclosure as Lewis number rises.
- The local fluxes calculated on the rectangular object have maxima in the neighborhoods of the corners. This happens due to separation of flow from corners.
- The influence of increasing Hartmann number on entropy generation and flow dynamics, enhanced convective heat transfer rates within the cavity.

**Conflict of interest:** The author(s) declare(s) that there is no conflict of interest regarding the publication of this paper.

**Data Availability Statement:** All relevant data include in the manuscript. There is no data to support the present work.

**Author Contributions**

**Conceptualization:** Shafee Ahmad **Formal analysis:** Hameed Ullah Jan, Bashir Shah **Investigation:** Hameed Ullah Jan **Methodology:** Waris Khan, **Software:** Waris Khan , **Writing - original draft:** Siddeeq Ahmad, Zeeshan Khan **Revision:** Zeeshan Khan, **Validation:** Shafee Ahmad, Bashir Shah

**Funding:** The authors present their appreciation to King Saud University for funding this research through the Ongoing Research Funding program, (ORF-2025-145), King Saud University, Riyadh, Saudi Arabia.

**References**

[1] S. U. S. Choi. Enhancing thermal conductivity of fluids with nanoparticles, *Developments and Applications of Non Newtonian Flows*. 231/MD : 99-105 (1995).

[2] K. Khanafer, K. Vafai, and M. Lightstone. Buoyancy-driven heat transfer enhancement in a two dimensional enclosure utilizing nanofluids. *International Journal of Heat and Mass Transfer*. 46 : 3639-3653 (2003).

[3] Lee, M., Kim, H. J., & Kim, D. K. (2016). Nusselt number correlation for natural convection from vertical cylinders with triangular fins. *Applied Thermal Engineering*, 93, 1238-1247.

[4] Senapati, J. R., Dash, S. K., & Roy, S. (2016). Numerical investigation of natural convection heat transfer over annular finned horizontal cylinder. *International Journal of Heat and Mass Transfer*, 96, 330-345.

[5] Hosseini, S. S., Ramiar, A., & Ranjbar, A. A. (2019). The effect of fins shadow on natural convection solar air heater. *International Journal of Thermal Sciences*, 142, 280-294.

[6] Shahabadi, M., Mehryan, S. A. M., Ghalambaz, M., & Ismael, M. (2021). Controlling the natural convection of a non-Newtonian fluid using a flexible fin. *Applied Mathematical Modelling*, 92, 669-686.

[7] Hatami, M., Zhou, J., Geng, J., Song, D., & Jing, D. (2017). Optimization of a lid-driven T-shaped porous cavity to improve the nanofluids mixed convection heat transfer. *Journal of Molecular Liquids*, 231, 620-631.

[8] Dash, R. K., K. N. Mehta, and G. Jayaraman. "Casson fluid flow in a pipe filled with a homogeneous porous medium." *International Journal of Engineering Science* 34.10 (1996): 1145-1156.

[9] Bejan, A. (1979). A study of entropy generation in fundamental convective heat transfer.

[10] Bejan, A. (1982). Second-law analysis in heat transfer and thermal design. In *Advances in heat transfer* (Vol. 15, pp. 1-58). Elsevier.

[11] Nakonieczny, K. (2002). Entropy generation in a diesel engine turbocharging system. *Energy*, 27(11), 1027-1056.

- [12] Maveety, J. G., & Razani, A. (1996). A two-dimensional numerical investigation of the optimal removal time and entropy production rate for a sensible thermal storage system. *Energy*, 21(12), 1265-1276.
- [13] Johannessen, E., & Kjelstrup, S. (2004). Minimum entropy production rate in plug flow reactors: An optimal control problem solved for SO<sub>2</sub> oxidation. *Energy*, 29(12-15), 2403-2423.
- [14] Basak, T., Kaluri, R. S., & Balakrishnan, A. R. (2011). Effects of thermal boundary conditions on entropy generation during natural convection. *Numerical Heat Transfer, Part A: Applications*, 59(5), 372-402.
- [15] Agbaje TM, Baithalu R, Mishra SR, Panda S. Irreversibility Processes on the Squeezing Flow Analysis of Blood-Based Micropolar Hybrid Nanofluid Through Parallel Channel: Spectral Quasilinearisation Method. *BioNanoScience*. 2024 May 3:1-5.
- [16] Panda S, Pattnaik PK, Baithalu R, Mishra SR. Inertial drag combined with non-uniform heat generation/absorption effects on the hydromagnetic flow of polar nanofluid over an elongating permeable surface due to the impose of chemical reaction. *ZAMM-Journal of Applied Mathematics and Mechanics/Zeitschrift für Angewandte Mathematik und Mechanik*. 2024:e202301058.
- [17] Baithalu R, Panda S, Pattnaik PK, Mishra SR. Blood-Based CNT Nanofluid Flow Over Rotating Discs for the Impact of Drag Using Darcy–Forchheimer Model Embedding in Porous Matrix. *International Journal of Applied and Computational Mathematics*. 2024 Jun;10(3):1-20.
- [18] Jan A, Mushtaq M, Hussain M. Heat transfer enhancement of forced convection magnetized cross model ternary hybrid nanofluid flow over a stretching cylinder: non-similar analysis. *International Journal of Heat and Fluid Flow*. 2024 Apr 1;106:109302.
- [19] Sudarsana Reddy, P., & Sreedevi, P. (2021). Entropy generation and heat transfer analysis of magnetic hybrid nanofluid inside a square cavity with thermal radiation. *The European Physical Journal Plus*, 136(1), 1-33.
- [20] Jan A, Mushtaq M, Hussain M. Heat transfer enhancement of forced convection magnetized cross model ternary hybrid nanofluid flow over a stretching cylinder: non-similar analysis. *International Journal of Heat and Fluid Flow*. 2024 Apr 1;106:109302.
- [21] Dutta, S., Goswami, N., Biswas, A. K., & Pati, S. (2019). Numerical investigation of magnetohydrodynamic natural convection heat transfer and entropy generation in a rhombic enclosure filled with Cu-water nanofluid. *International Journal of Heat and Mass Transfer*, 136, 777-798.
- [22] Bondareva, N. S., Sheremet, M. A., Oztop, H. F., & Abu-Hamdeh, N. (2016). Heatline visualization of MHD natural convection in an inclined wavy open porous cavity filled with a nanofluid with a local heater. *International Journal of Heat and Mass Transfer*, 99, 872-881.



[23] Sheikholeslami, M., & Shehzad, S. A. (2017). RETRACTED: Magnetohydrodynamic nanofluid convective flow in a porous enclosure by means of LBM.

[24] Muthukumar, S., Sureshkumar, S., Chamkha, A. J., Muthamilselvan, M., & Prem, E. (2019). Combined MHD convection and thermal radiation of nanofluid in a lid-driven porous enclosure with irregular thermal source on vertical sidewalls. *Journal of Thermal Analysis and Calorimetry*, 138, 583-596.

[25] Gireesha, B. J., et al. "Entropy generation and heat transport analysis of Casson fluid flow with viscous and Joule heating in an inclined porous microchannel." *Proceedings of the Institution of Mechanical Engineers, Part E: Journal of Process Mechanical Engineering* 233.5 (2019): 1173-1184.

[26] Sohail, Muhammad, et al. "Entropy generation in MHD Casson fluid flow with variable heat conductance and thermal conductivity over non-linear bi-directional stretching surface." *Scientific Reports* 10.1 (2020): 12530.

[27] Kotha, Gangadhar, and Ali J. Chamkha. "Entropy generation on convectively heated surface of casson fluid with viscous dissipation." *Physica Scripta* 95.11 (2020): 115203.

[28] Shaw, Sachin, et al. "Impact of entropy generation and nonlinear thermal radiation on Darcy–Forchheimer flow of  $MnFe_2O_4$ -Casson/water nanofluid due to a rotating disk: Application to brain dynamics." *Arabian Journal for Science and Engineering* 45 (2020): 5471-5490.

[29] Adebayo, Olusegun, et al. "Numerical simulation of entropy generation for casson fluid flow through permeable walls and convective heating with thermal radiation effect." *Journal of the Serbian Society for Computational Mechanics/Vol 14.2* (2020): 150-167.

[30] Pattnaik PK, Baithalu R, Mishra SR, Panda S. Effective thermal properties under the influence of various shapes of the nanoparticles on the flow of ternary hybrid nanofluid over an infinite vertical plate. *Pramana*. 2024 Jul 23;98(3):104.

[31] Panda S, Baag AP, Pattnaik PK, Baithalu R, Mishra SR. Artificial neural network approach to simulate the impact of concentration in optimizing heat transfer rate on water-based hybrid nanofluid under slip conditions: A regression analysis. *Numerical Heat Transfer, Part B: Fundamentals*. 2024 Mar 25:1-23.

[32] Baithalu R, Mishra SR. On the free convection of magneto-micropolar fluid in association with thermal radiation and chemical reaction and optimized heat transfer rate using response surface methodology. *Modern Physics Letters B*. 2023 Nov 30;37(33):2350171.

[33] N. Ahmed, U. Khan, S.I. Khan, S. Bano, and S.T. Mohyud-Din, "Effects on magnetic field in squeezing flow of a Casson fluid between parallel plates," *Journal of King Saud University-Science*, vol. 29, no. 1, pp. 119-125, Jan 2017. DOI: 10.1016/j.jksus.2015.03.006.

[34] J.V.R. Reddy, V. Sugunamma, and N. Sandeep, "Enhanced heat transfer in the flow of dissipative non-Newtonian Casson fluid flow over a convectively heated upper surface of a paraboloid of revolution," *Journal of Molecular liquids*, pp. 229, pp. 380-388, March 2017. DOI: 10.1016/j.molliq.2016.12.100.

- [35] Baithalu R, Mishra SR. On optimizing shear rate analysis for the water-based CNT micropolar nanofluids via an elongating surface: response surface methodology combined with ANOVA test. *Journal of Thermal Analysis and Calorimetry*. 2023 Dec;148(24):14275-94.
- [36] Shamshuddin, M. D., and W. Ibrahim. "Finite element numerical technique for magneto-micropolar nanofluid flow filled with chemically reactive Casson fluid between parallel plates subjected to rotatory system with electrical and Hall currents." *International Journal of Modelling and Simulation* 42.6 (2022): 985-1004.
- [37] Goud, B. Shankar, P. Pramod Kumar, and Bala Siddulu Malga. "Effect of heat source on an unsteady MHD free convection flow of Casson fluid past a vertical oscillating plate in porous medium using finite element analysis." *Partial Differential Equations in Applied Mathematics* 2 (2020): 100015.
- [38] Majeed, Afraz Hussain, et al. "Heat and mass transfer characteristics in MHD Casson fluid flow over a cylinder in a wavy channel: Higher-order FEM computations." *Case Studies in Thermal Engineering* (2023): 102730.
- [39] Khader, M. M., Mustafa Inc, and Ali Akgul. "Numerical appraisal of the unsteady Casson fluid flow through Finite Element Method (FEM)." *Scientia Iranica* 30.2 (2023): 454-463.
- [40] Kumar, BV Rathish, and Manisha Chowdhury. "Multiscale stabilized finite element computation of the non-Newtonian Casson fluid flowing in double lid-driven rectangular cavities." *Computers & Mathematics with Applications* 143 (2023): 57-72.
- [41] Zhao, F.Y., Liu, D. and Tang, G.F., 2007. Conjugate heat transfer in square enclosures. *Heat and mass transfer*, 43(9), pp.907-922.
- [42] Liu, D., Zhao, F.Y. and Tang, G.F., 2007. Conjugate heat transfer in an enclosure with a centered conducting body imposed sinusoidal temperature profiles on one side. *Numerical Heat Transfer, Part A: Applications*, 53(2), pp.204-223.
- [43] Chamkha, A.J. and Ismael, M.A., 2013. Conjugate heat transfer in a porous cavity filled with nanofluids and heated by a triangular thick wall. *International Journal of Thermal Sciences*, 67, pp.135-151.
- [44] Ismael, M.A. and Chamkha, A.J., 2015. Conjugate natural convection in a differentially heated composite enclosure filled with a nanofluid. *Journal of porous media*, 18(7).
- [45] Garoosi, F. and Talebi, F., 2017. Numerical analysis of conjugate natural and mixed convection heat transfer of nanofluids in a square cavity using the two-phase method. *Advanced Powder Technology*, 28(7), pp.1668-1695.
- [46] Mehryan, S.A.M., Ghalambaz, M. and Izadi, M., 2019. Conjugate natural convection of nanofluids inside an enclosure filled by three layers of solid, porous medium and free nanofluid using Buongiorno's and local thermal non-equilibrium models. *Journal of Thermal Analysis and Calorimetry*, 135, pp.1047-1067.
- [47] Kolsi, L. (2016). Numerical study of natural convection and entropy generation of Al<sub>2</sub>O<sub>3</sub>-water nanofluid within a cavity equipped with a conductive baffle. *Journal of Applied Fluid Mechanics*, 9(5), 2177-2186.

[48] Jan A, Mushtaq M, Hussain M. Nonsimilar analysis of forced convection radially magnetized ternary hybrid nanofluid flow over a curved stretching surface. Numerical Heat Transfer, Part B: Fundamentals. 2024 May 10:1-29.

[49] Farooq U, Irfan M, Khalid S, Jan A, Hussain M. Computational convection analysis of second grade MHD nanofluid flow through porous medium across a stretching surface. ZAMM-Journal of Applied Mathematics and Mechanics/Zeitschrift für Angewandte Mathematik und Mechanik. 2024 Apr;104(4):e202300401.

**Nomenclature**

FEM= finite element method

$u,v$  = nondimensional velocities components

$p$ =nondimensional pressure

$c$  = concentration

$\theta$ = nondimensional temperature

$\beta$ = Casson parameter

$R_k$ = Thermal conductivity ratio

$Ha$ = Hartmann number

$Ra$ = Rayleigh number

$Le$ = Lewis number

$Da$ = Darcy number

$\gamma$ = magnetic field inclination

$Pr$  = Prandtl number

$Nu$ = local Nusselt number

$Sh$ = local Sherwood number

$K.E.$  = total kinetic energy

$Nu_{avg}$ = mean Nusselt number

$Sh_{avg}$ = mean Sherwood number

$K.E._{avg}$  = mean total kinetic energy